

Why does necking ignore notches in dynamic tension?

*Y. Rotbaum, S. Osovski and D. Rittel**

Faculty of Mechanical Engineering, Technion, 32000 Haifa, Israel

Abstract

Recent experimental work has revealed that notched tensile specimens, subjected to dynamic loading, may fail by growing a neck outside of the notched region. This apparent lack of sensitivity to a classical stress concentration case was reported but not explained or modeled.

The present paper combines experimental and numerical work to address this issue. Specifically, it is shown that the dynamic tensile failure locus is dictated by both the applied velocity boundary condition and the material mechanical properties, specifically strain-rate sensitivity and strain-rate hardening.

It is shown that at sufficiently high impact velocities, the flows stress in the notch vicinity becomes quite higher than in the rest of the specimen, so that while the former resists deformation, it transfers the load to the latter. The result will be the formation of a local neck and failure away from the notch.

This effect is shown to be active when the material properties are perturbed only at the local level, as in the case of machining of the notch, which in itself may again be sufficient to stabilize the structure under local failure until a neck forms elsewhere.

While the physical observations are quite counterintuitive with respect to the engineering views of stress concentrator's effect, the present work rationalizes those observations and also provides information for the designers of dynamically tensioned structures that may contain notches or similar flaws.

Keywords: Necking, Ductility, Kolsky-bar, Notch, Strain-rate hardening

(*) Corresponding author: merittel@technion.ac.il

Introduction

The mechanical response of a structural element under external loads may be strongly influenced by the presence of geometrical discontinuities such as fillets, grooves, threads, or alike. The local geometrical perturbation (or discontinuity) amounts to a local increase in the stress field surrounding it. The role of stress concentrators on the deformation process is of prime importance in the field of mechanical design. Classical works, which are constantly used by structural engineers, can be found in [1-4], where the emphasis is mostly on elastic stress concentration problems. The importance of notched members under tension has led to a vast body of works focusing on evaluating the stress intensity factors around geometrical discontinuities [5-8], and specifically the differences between quasi-static and dynamic loading scenarios [9-11].

An underlying assumption in all of the above-mentioned studies is that the fracture locus will be that of the geometrical imperfection, or any other given flaw. The same assumption is implicitly extended to dynamic loading situations, where inertia plays an important role. Other material heterogeneities related to the manufacturing process are ignored in the vast majority of works, or are considered secondary with respect to the presence of the dominant flaw.

It was recently shown that under dynamic loading conditions, the location of neck in a smooth bar subjected to tensile loading, is a deterministic event resulting from the applied boundary conditions [12]. Furthermore, it was shown experimentally that the necking location, as dictated by the applied boundary conditions, may prevail even in the presence of a geometrical perturbation which was deliberately introduced as a notch. The results of Rittel et al. [13] imply that the presence (or pre-assumption) of a structural flaw, cannot be considered as the dominant factor in determining the locus of the dynamic structural failure. In other

words, those results show that *the presence of a geometrical imperfection will not necessarily dictate the dynamic failure locus, as commonly assumed in the literature.*

Therefore, one standing issue is the identification of the physical factors controlling the dynamic failure locus in the presence of a geometrical imperfection. In consistence with our previous work [13], the geometrical imperfection considered here is a notch, rather than the usual smooth variations of a characteristic dimension (e.g. diameter) found in the literature [14] and references within.

The present study, of a hybrid experimental-numerical character, examines several potent factors responsible for the selection of the dynamic failure locus, as follows.

First, the methods used for the above-mentioned investigation are detailed. The experimental setup used for the dynamic tests, as well as the tested materials and specimens' geometry are described, followed by a detailed description of the numerical model used to study the potential factors. The experimental results are then presented, from which a critical notch size is extracted. The critical notch size is defined as the notch depth for which the majority of the specimens fail statically, within the notch. Next, new results for dynamic tensile tests of notched 15-5 PH (annealed) and 4340 steel specimens are presented. Finally numerical simulations are used to examine the role of the material's rate dependence as well as the local hardening stemming from the manufacturing process on the competition between the potential failure sites. We then discuss and summarize the main findings of this work.

Experimental setup

a. Materials and specimens

Two materials were tested: 15-5 PH steel (condition A) and 4340 H&T, supplied as 12.7[mm] diameter bars, and tested in the as-received condition. Tensile cylindrical specimens with end

threads were machined from the bars. The dimensions of the specimen are shown in Figure 1. A summary of the characteristic dimensions used for static and dynamic tests is presented in Table 1. For the dynamic tensile experiments, two types of specimens were manufactured, namely long (36 [mm] gauge length), and short (12 [mm] gauge length) specimens, both having a diameter of 3 [mm]. In addition, the specimens were grooved circumferentially, using a machining thread tool knife, to a specific depth and geometry as listed in Table 2. Note that, while the dynamic specimens were notched at mid-gauge length, the static ones were notched at 1/3 of the length to avoid any possible confusion with potential symmetrical failure (necking).

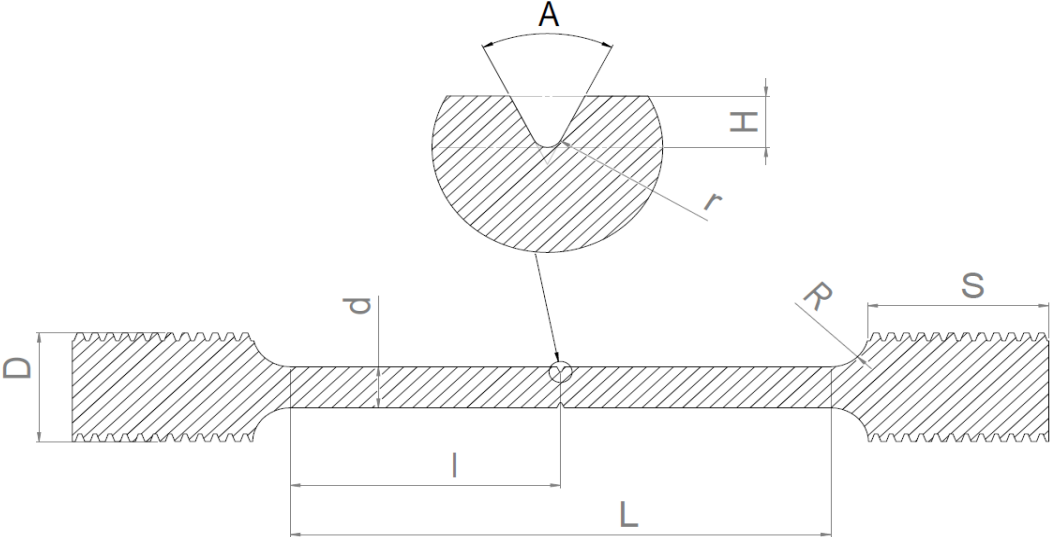


Figure 1. Static and dynamic tensile specimens' geometry.

Experiment type	S [mm]	R [mm]	D [mm]	d [mm]	L [mm]	l [mm]
Dynamic	12	2.5	7.953	3	36 & 12	18 & 6
Static	12	2.5	7.953	3	36	12

Table 1. Static and dynamic tensile specimens' characteristic dimensions (mm), as defined in Figure 1.

Material	A [deg]	r [mm]	$\frac{H_{critical}}{d}$
PH 15-5 condition A	55 ⁰	0.04	10%
4340 H&T steel	55 ⁰	0.04	10%

Table 2. Characteristic notch dimensions for each material.

Material	$\frac{H_{critical}}{d}$	Number of Tensile samples	Strain rate [1/s]
PH 15-5 (condition A)	10%	50	200-2000
4340 H&T	10%	40	200-2000

Table 3. Specimens used for dynamic experiments and experimental conditions.

A total of 90 specimens were tested to ensure repeatability of the results. In addition we tested 40 specimens of 7075-T6 aluminum alloy. Those yielded the same qualitative results as those reported in the sequel, and therefore will not be presented here for the sake of brevity.

b. Static tensile testing

The static tensile tests were conducted on a servo-hydraulic testing machine MTS 810 under displacement control, with a prescribed crosshead velocity of 2.64 [mm / min]. A laser extensometer (LE-05, EIR) was used for the longitudinal strain measurements.

c. Dynamic tensile Hopkinson setup

The dynamic tension specimens were tested in a standard 12.7 [mm] diameter Kolsky tensile apparatus [15, 16] made of C300 hardened Maraging steel bars. The apparatus was loaded

using a 400[mm] long tubular projectile, launched toward a flange located at the end of the incident bar. In order to ensure wave separation, a momentum trap was brought initially in contact with the loaded flange of the incident bar, whose length was identical to that of the projectile bar, as shown in Figure 2.

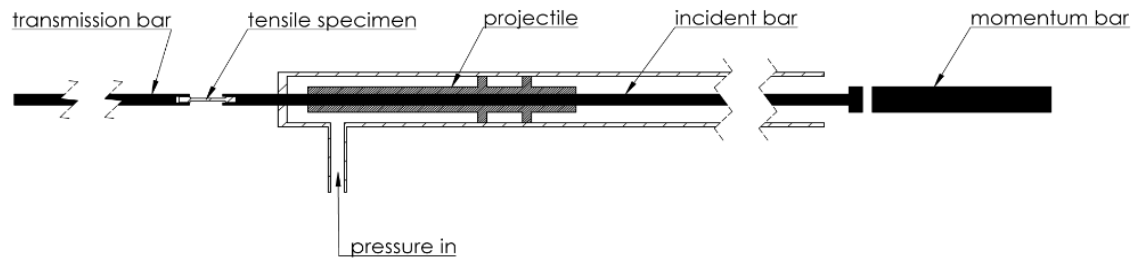


Figure 2. Schematic representation of the Kolsky tension apparatus.

A Cordin 530 high speed camera (HSC) and a Kirana high speed digital camera were synchronized with the incident bar signals to capture the evolution of the specimens' macroscopic deformation, including the onset and evolution of localization.

Finite elements analysis

Finite elements model

The dynamic tensile tests were modeled using the commercial finite element package Abaqus explicit [17]. The geometrical model included the entire tensile apparatus with the exception of the stopper and the momentum bar. In order to reduce computation time the lengths of the incident bar was shorten to a total length of 0.8[m]. The meshing was done using a 4-node bilinear axisymmetric quadrilateral elements (CAX4R) with reduced integration and hourglass control. The element size in the specimen's gauge was taken to be 20[μm] and a total of 200,114 elements were used. Convergence of the numerical solution

with respect to the element size within the gauge was verified. The uniform mesh size was chosen so as to minimize the effect of the mesh on the localization locus.

The boundary conditions used in the simulations, were set as a symmetrical trapezoidal velocity profile with a maximum amplitude, denoted as V_{\max} in the range of $7-21[m/s]$, and a characteristic rise time of $36[\mu\text{sec}]$. The velocity profile was applied on the free surface of the incident bar. The entire pulse duration was set as $200[\mu\text{sec}]$, similar to the experimental pulse. (Figure 3).

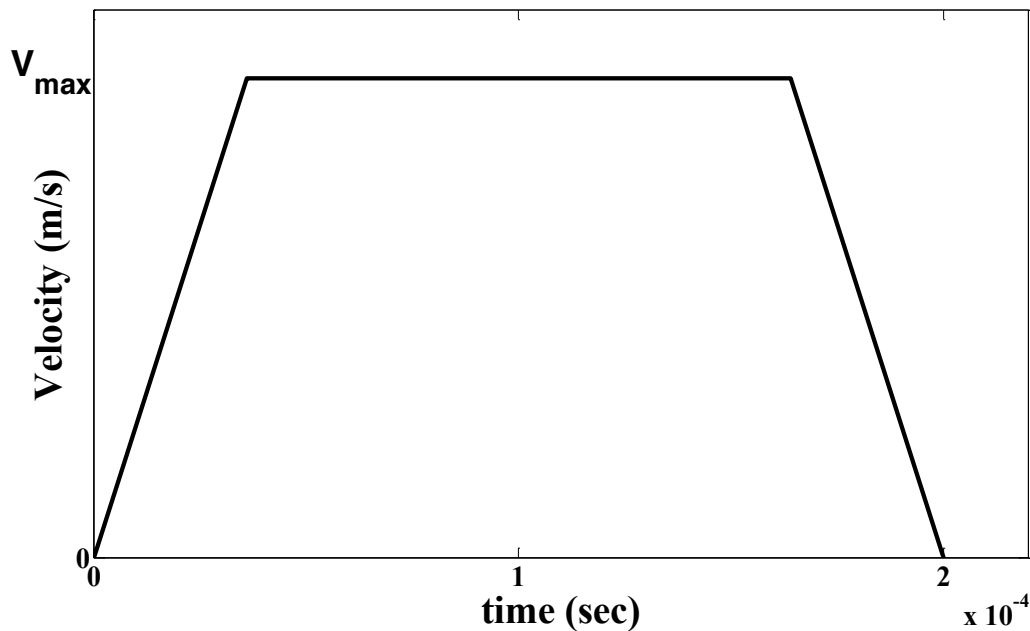


Figure 3. Typical velocity profile used as B.C for the simulations.

Material model

The response of the elastic viscoplastic material is calculated within the framework of J_2 flow theory and the symmetric part of the total strain increment is assumed to be additively decomposed into an elastic and viscoplastic part. The plastic strain rate $\dot{\epsilon}$ is given by

$$\dot{\varepsilon} = R \left[\frac{\bar{\sigma}}{g(\varepsilon_p)} \right] \quad (1)$$

$$g(\varepsilon_p) = \sigma_0 \left[1 + \varepsilon_p / \varepsilon_0 \right]^n \quad (2)$$

with $\varepsilon_p = \int \dot{\varepsilon} dt$ and $\varepsilon_0 = \sigma_0 / E$, while $\bar{\sigma}$ is the flow stress. σ_0 is the yield stress, E is the Young's modulus and n is the strain hardening exponent. As in Zhou et al. (1994) [18], the function R(x) is used to account for increased rate sensitivity at high strain rates (Figure 4) and is given by:

$$R(x) = \frac{\dot{\varepsilon}_1(x) \dot{\varepsilon}_2(x)}{\dot{\varepsilon}_1(x) + \dot{\varepsilon}_2(x)} \quad (3)$$

$$x = \frac{\bar{\sigma}}{g(\varepsilon_p)} \quad (4)$$

Where $\dot{\varepsilon}_1$ is given by

$$\dot{\varepsilon}_1(x) = \dot{\varepsilon}_0(x)^{1/m} \quad (5)$$

Where m is the strain rate hardening exponent, and $\dot{\varepsilon}_2$ is given by

$$\dot{\varepsilon}_2(x) = \dot{\varepsilon}_m \exp \left[-\frac{a}{x} \right] \quad (6)$$

The rate formulation given in Eq. 3 insures a smooth transition between the viscoplastic responses at the two strain rate regimes.

Four specific set of values the parameters a and $\dot{\varepsilon}_m$ were considered, and will be labeled subsequently as cases 1-4, As listed in Table 4.

Case	a	$\dot{\epsilon}_m$ [s^{-1}]
1	6.7	5e6
2	3.4	2e5
3	6	5e6
4	2.6	2e5

Table 4. The 4 cases (sets) of material parameters used in the numerical simulations.

Note that the material properties used in the simulations are of a generic character and do not represent accurately the experimental materials of the study. As such, they are used to explore trends and not reproduce experimental results. The normalized flow stress vs. the plastic strain rate calculated for cases 1-4 are shown in Figure 4 (a-b).

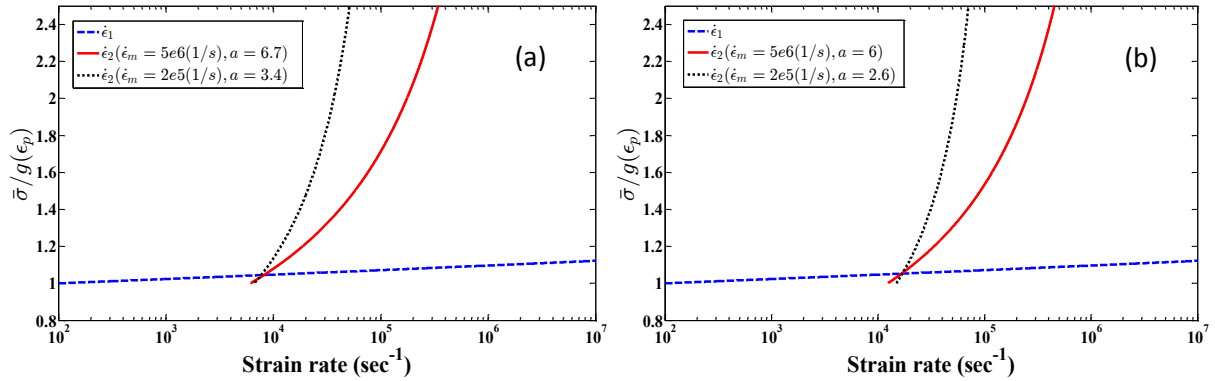


Figure 4. Normalized flow strength $\bar{\sigma} / g(\epsilon_p)$ versus plastic strain rate $\dot{\epsilon}$. (a) Calculated with the set of parameters of case 1 and case 2. (b) Calculated with the set of parameters of case 3 and case 4.

The material parameters were taken as characteristic of steel: $\rho = 7780 [Kg / m^3]$,

$E = 200 [GPa]$, $\nu = 0.3$, $\sigma_0 = 970 [MPa]$, $n = 0.01-0.15$, $m = 0.01-0.02$, $\dot{\epsilon}_0 = 100 [s^{-1}]$,

$\dot{\epsilon}_m = 2e5 - 5e6 [s^{-1}]$, and $a = 2.6-6.7$.

Experimental results

Static tensile experiments

To determine the notch size to be used for the dynamic experiments, a set of static tensile experiments were conducted on notched specimens with a notch relative depth, ranging from 1-10% of the cross section diameter. The aim of those preliminary static tests, was to identify a groove size which will be large enough to ensure that failure occurs within the notch, as reported in[13]. In Figures 5 (a) and (b), the effect of a 10% groove is shown for 15-5 PH steel and 4340 steel respectively.

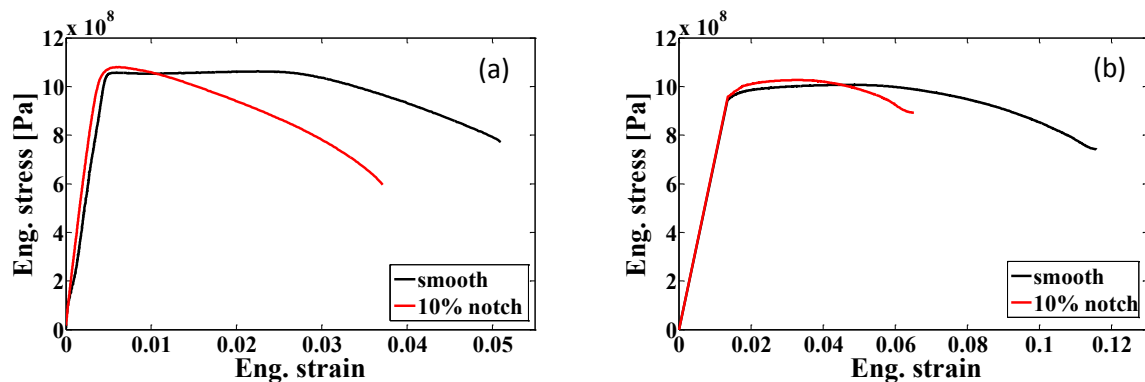


Figure 5. Typical engineering stress-strain curves comparing a smooth and a 10% notched specimen. (a) 15-5 PH steel. (b). 4340 steel. Both experiments were held with a constant cross head velocity of $2.64 [mm / min]$. (Nominal strain rate of $10^{-3} [1 / s]$).

As evident from Figures 5, a 10% notch has a substantial effect on the structural response to the static tensile loading in both tested materials. The total elongation up to fracture decreases due to the localization of deformation in the notch, leading to early failure at the same location. One should also note that for the notched specimens the flow stress seems to increase, which might be the result of notch strengthening[19, 20]. Note that, throughout this work, stresses are reported as engineering (nominal) to allow for comparison of the overall

specimen responses, including the inhomogeneous deformation state. Therefore, the selected critical notch size was 10%.

Dynamic tensile experiments

A basic demand for dynamic experiments is that *force equilibrium* must prevail during the dynamic tensile process. It was already shown that long tensile specimens are capable of reaching such force equilibrium [21], however the effect of the notch on the equilibrium was not previously examined before. Typical force equilibrium of a 10% notch sample is shown in Figure 6 for 4340 steel at a nominal strain rate of $650 [s^{-1}]$. This figure shows that specimen equilibrium is not at all affected by the presence of the notch, just as observed previously for long smooth specimens.

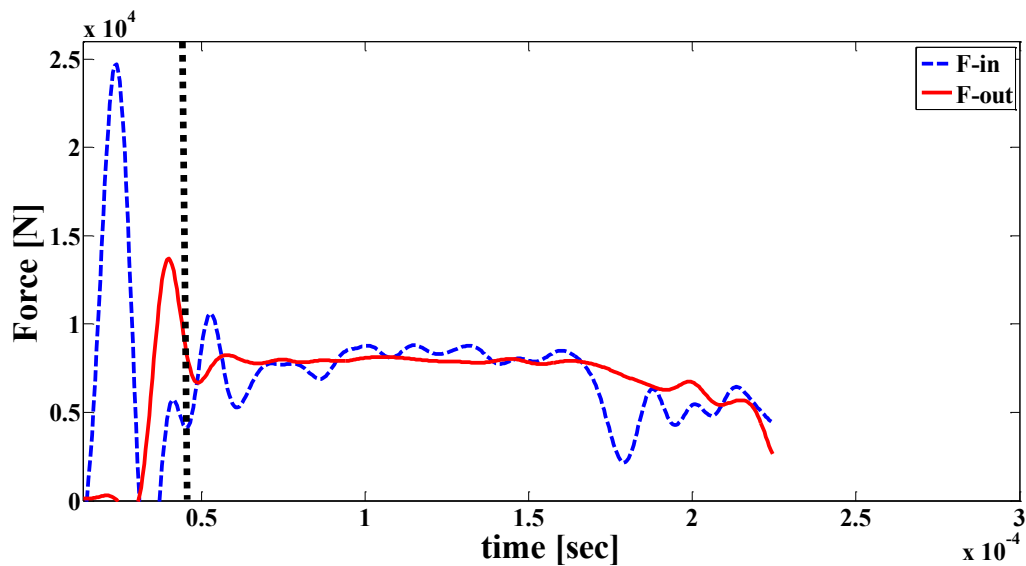


Figure 6. Typical force profiles recorded on the 10% notched specimens' edges (F_{in} , F_{out}) for 4340 steel strained at a rate of $650 [s^{-1}]$. Force equilibrium is observed over a large part of the loading process.

Let us consider now the relation between the presence of a notch and the failure location. While for quasi-static loading it was shown that specimens will always fail at the same location as the notch (for a 10% notch), a very different picture is revealed for specimens loaded dynamically as can be seen in Table 4, where the failure location of 13 representative dynamically loaded notched specimens is presented. Note that the impacted side refers to the side which is first loaded by the stress wave. To better understand the relation between loading velocity and subsequent necking location the reader is referred to [12].

Specimen number	Material	Gauge length [mm]	Strain rate [s^{-1}]	Failure location
1	4340 steel	36	450	Opposite
2	4340 steel	36	500	Opposite
3	4340 steel	36	540	Impacted
4	4340 steel	12	650	Opposite
5	4340 steel	12	730	Notch + opposite
6	4340 steel	12	890	Notch
7	15-5 PH steel	36	420	opposite
8	15-5 PH steel	36	450	Notch
9	15-5 PH steel	36	540	Opposite
10	15-5 PH steel	36	520	Impacted
11	15-5 PH steel	12	950	Notch
12	15-5 PH steel	12	600	Opposite
13	15-5 PH steel	12	750	Opposite

Table 5. Representative experimental results of dynamic tension experiments.

This experimental phase included 50 samples of PH 15-5 steel, 40 samples of 4340 steel, and 40 samples made of 7075-T6 aluminum alloy.

Nine typical frames captured during a dynamic experiment (specimen 9 in Table 5) are presented in Figure 7.

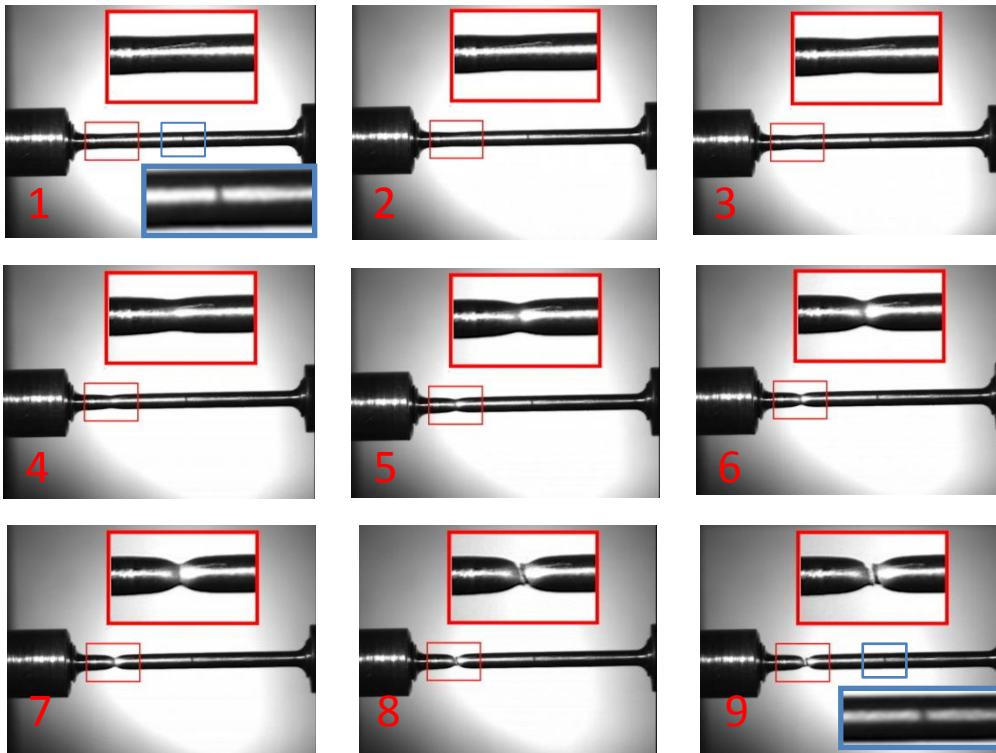


Figure 7. Geometrical evolution of specimen 9 made of PH 15-5 steel, loaded at a nominal strain rate of $540 [s^{-1}]$. Frame 1 corresponds to $t=100[\mu sec]$ and frames 2-9 are spaced $5 \mu sec$ apart. Even though a 10% notch was introduced at the center of the specimen, a neck develops into fracture, which occurs at $145 [\mu sec]$. Note that the notch gets barely deformed throughout the test.

From Figure 7 it is evident that most of the plastic deformation occurs outside of the notched region, at the same location where it was observed to occur for a smooth specimen subjected to the same boundary conditions [12]. The specimen tested here fractured at the same location, as indicated in Table 5, despite being notched.

Typical engineering stress-strain curves obtained for a smooth specimen and a specimen having a 10% notch and a gauge length of $36[mm]$ are compared in Figure 8(a-b) for

dynamically loaded 15-5 PH and 4340 steel specimens. The picture revealed by Figure 8 is remarkably different that presented in Figure 5 for the quasi-static case. Almost no difference is observed in the structural response of the two different specimens, supporting the visual findings in Figure 7 that the notch has a little, if any, effect if any on the deformation process.

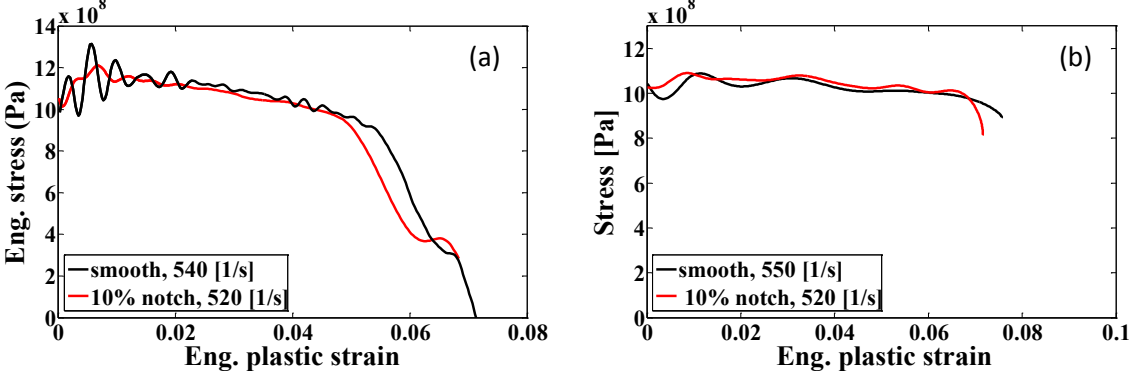


Figure 8. Typical engineering stress-strain curves comparing a smooth and a 10% notched steel specimen, both with a gauge length of 36 [mm]. (a) 15-5 PH steel. (b) 4340 steel.

In other words, the notch which is traditionally regarded as the weakest link does not act as such, suggesting the weakest link theory which is often used to describe the quasi-static loading case, fails when dynamic loading conditions are applied, at least for the ductile failure case at hand.

Let us consider now dynamic tensile experiments performed with short notched specimens. In this case, unlike for the longer specimens, some of the specimens actually broke in the notch. It is therefore interesting to consider overall specimen ductility in relation to the fracture locus, as shown in Figure 9. This figure shows that the overall ductility to failure is markedly influenced by the fracture locus. Specifically, early failure in the notch dramatically reduces the overall elongation to failure, as expected.

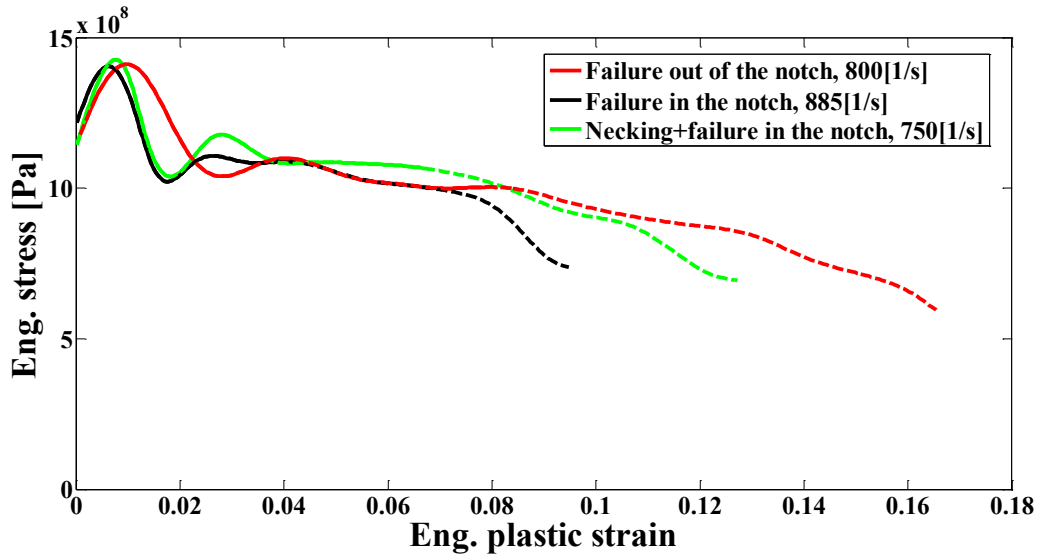


Figure 9. Typical engineering stress-strain curve comparing three 4340 steel specimens with a gauge length of 12 [mm].

Numerical Results

As mentioned before, the simulations presented below were performed with the following material parameters: $\rho = 7780 [Kg / m^3]$, $E = 200 [GPa]$, $\nu = 0.3$, $\dot{\epsilon}_0 = 100 [s^{-1}]$, $\sigma_0 = 970 [MPa]$, $n = 0.01$, and $m = 0.01$. The peak amplitude of $V_{striker}$ was in the range of 7–21 [m / s]. Note that for 17.5 [m / s], the nominal strain rate was $\sim 1000 [s^{-1}]$.

As shown in Figure 4, the parametric change of a and $\dot{\epsilon}_m$ controls the transition associated with the second strain rate regime [22]. The local strain-rate in the neck is approximately ten times higher than the nominal strain-rate of $1000 [s^{-1}]$, while the local strain rate at the notch root may reach up to $50000 [s^{-1}]$. The observed differences in strain rates between the two potential necking sites may have a rather large stabilizing effect on the neck development

under the notch, as evident from [23-25], where the effect of strain rate on necking instability was examined.

Representative results of the numerical simulations of smooth and 10% center-notched samples, stretched at a peak velocity of 17.5 [m/s], are shown in Figure 10.

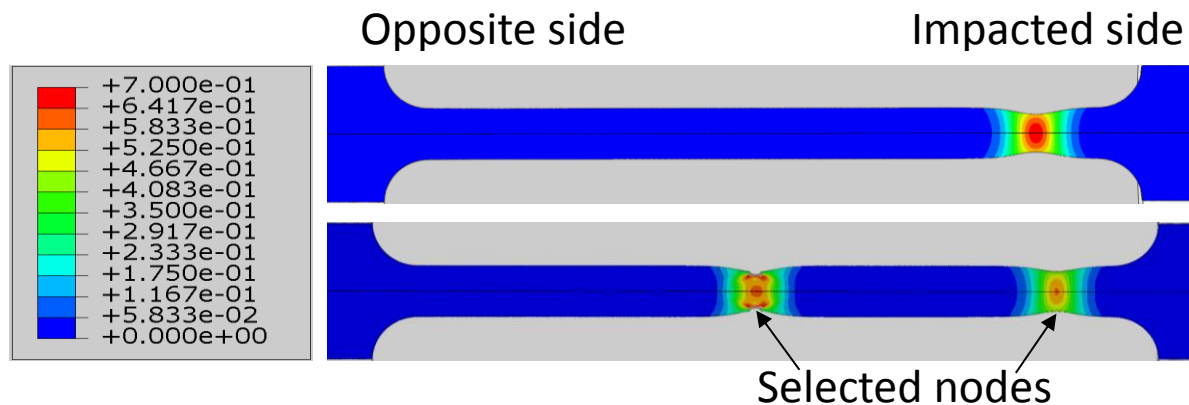


Figure 10. Numerical simulation of dynamically deformed representative steel specimens stretched at a peak velocity of 17.5 [m/s]. The upper specimen is smooth while the lower contains a 10% notch. The color map represents the equivalent plastic strain values. Here, ϵ_m and $\dot{\epsilon}_m$ values are those of case 1.

For a smooth specimen, the failure location is on the impacted side, in correspondence with [12]. For the notched specimen, one observes a strong competition between the neck on the impacted side and the imperfection in the middle of the gauge. This is the outcome of the joint influence of inertia and stress waves against local the stress concentration. This competition will be addressed in detail in the sequel.

Since damage and subsequent failure are not accounted for by the numerical model, the failure location is determined by the local radial displacement (U_1) which serves as a geometrical indicator for the radial neck and notch growth. For this purpose, two points are selected, as shown in Figure 10. The failure time is synchronized with respect to time at which the stress wave impinges upon the specimen.

An example for the behavior of U_1 for three different V_{striker} amplitudes (10.0, 18.5 and 20.5[m/s]) is presented in Figure 11 a-c, respectively.

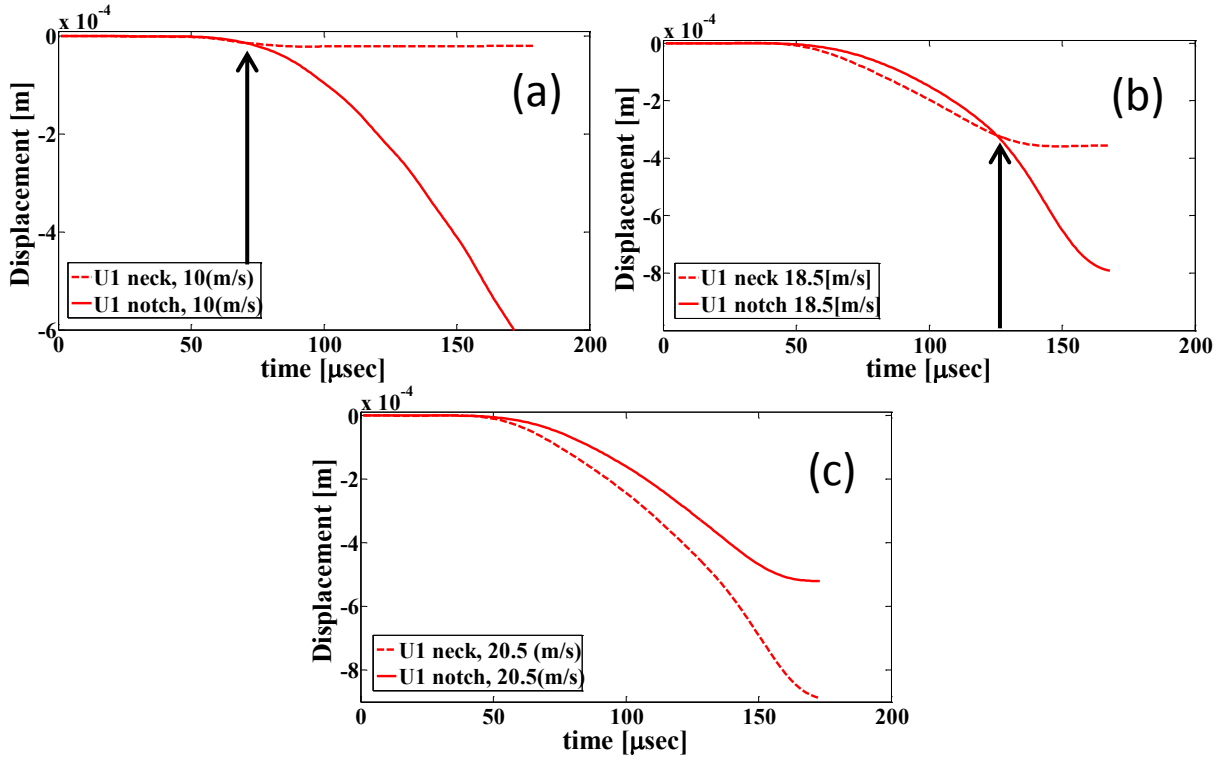


Figure 11. Evolution of u_1 displacement value at the potential failure sites. This figure illustrates the competition between the potential failure sites. (a) $V_{\text{max}} = 10[m / s]$. (b) $V_{\text{max}} = 18.5[m / s]$. (c) $V_{\text{max}} = 20.5[m / s]$. Note the evolution of the meeting point which disappears at the highest velocity. Here, a and $\dot{\epsilon}_m$ values are those of case 1.

For the lower velocity, $V_{\text{max}} = 10[m / s]$, the displacement (U_1), is equal in the notch and in the neck, at the early stages until $t=70[\mu\text{sec}]$, and beyond that time, the notch grows faster than the neck. When $V_{\text{max}} = 18.5[m / s]$, there is a clear competition between the localized sites, therefore the U_1 amplitudes become equal (meeting time) after a longer time, of the

order of $t=123[\mu\text{sec}]$. Finally, for $V_{\text{max}} = 20.5[m/s]$, although the two potential sites deform significantly, the radial displacement of the neck is greater at all times, indicating that this will be the failure locus. The influence of the V_{max} amplitude on U_1 "meeting time" was examined over a wide range of velocities, and the change in the macroscopic elongation (EL_{tot}) as a function of V_{max} are plotted for each one of the parametric cases (Figure 12 a-b). Figure 12 a, presents case 1 and 2 (material parameters), for which the transition occurs at a comparable same strain rate of $8000[s^{-1}]$, but with a different slope of $\dot{\epsilon}_2$. Figure 12 b shows the same for cases 3 and 4, with a transition strain rate close to $16000[s^{-1}]$.

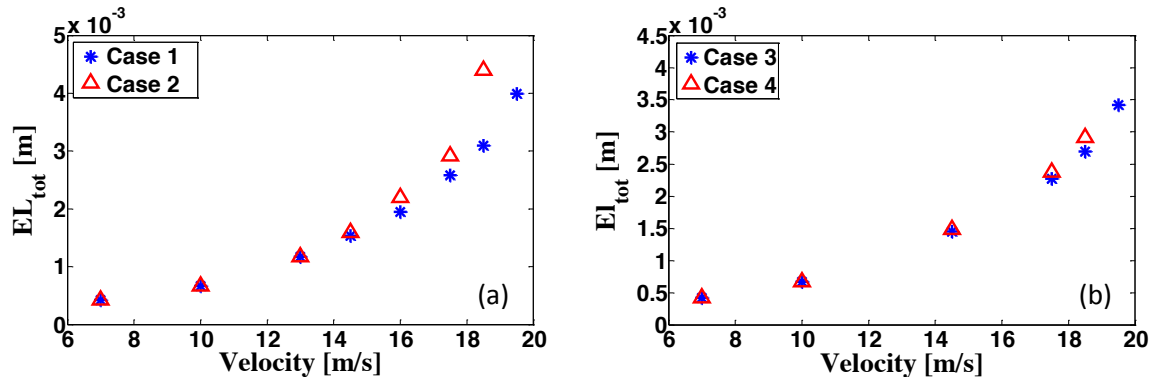


Figure 12. Macroscopic elongation (EL_{tot}) at equal radial displacement values (meeting time). (a) Cases 1 and 2. (b) Cases 3 and 4.

One should emphasize that the case with a higher "meeting time" for specific velocity amplitude (Fig. 12a) is more stable in the sense that larger total elongation to fracture can be reached. In other words the competition between the two localization area lasts longer. Comparing Figures 12 a and b shows that a lower transition strain rate between $\dot{\epsilon}_1$ and $\dot{\epsilon}_2$ stabilizes the structure, since for the early transition to $\dot{\epsilon}_2$, the hardening becomes significant at the notch tip, therefore restraining its deformation. A stronger slope after the transition strain rate (cases 2 or 4), has the same effect. The ability of the structure to undergo neck

retardation can be seen in the macroscopic stress-strain curves, as illustrated in Figure 13 for case 1.

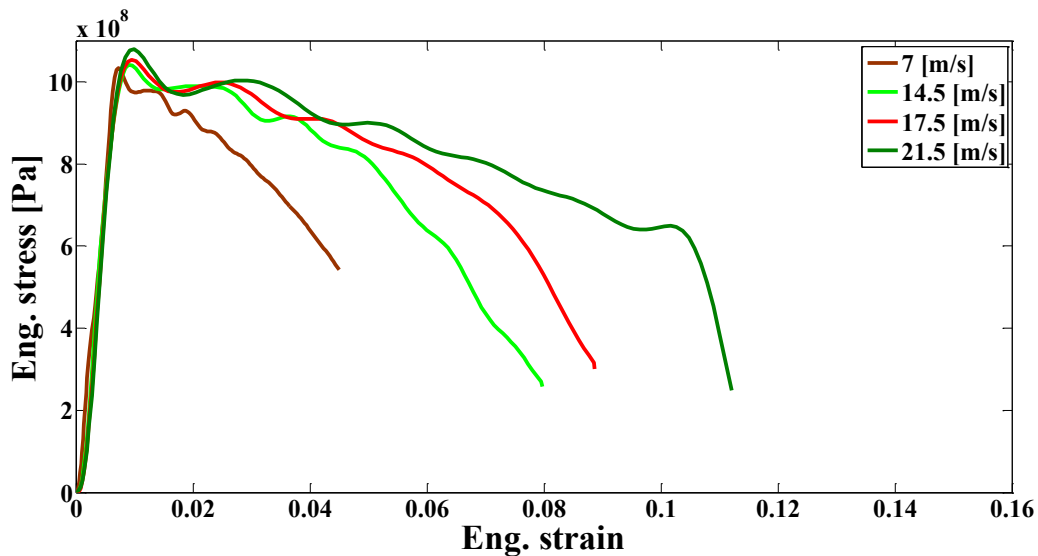


Figure 13. Calculated engineering stress-strain curves for case 1. Note that an increase of impact velocity tends to stabilize the structure.

This figure shows that for the low range of velocities $7 - 14.5 [m/s]$, the strain to failure is relatively low. This stems from the fact that the local strain rates are not sufficiently high to cause a significant notch-tip hardening. Further elevation in the velocity promotes the competition between the notch and the potential neck, conferring a higher energy absorbing capability to the specimen (toughness).

Notch machining considerations

An important issue, which is generally overlooked, concerns the machining of the notch. The latter has a definite local hardening effect, which can be somewhat mitigated by annealing treatments. The experimental results presented for the notched specimens, as well as those presented in [13], were for specimens that were not annealed after machining. An obvious consequence of the machining process is an increase in the yield strength due to strain hardening. Cold work also causes a general increase in the material's flow stress, as presented next.

To further illustrate the point, smooth specimens were machined with and without water cooling to assess, first, the overall influence of the manufacturing process on the quasi-static tensile properties (Figure 14).

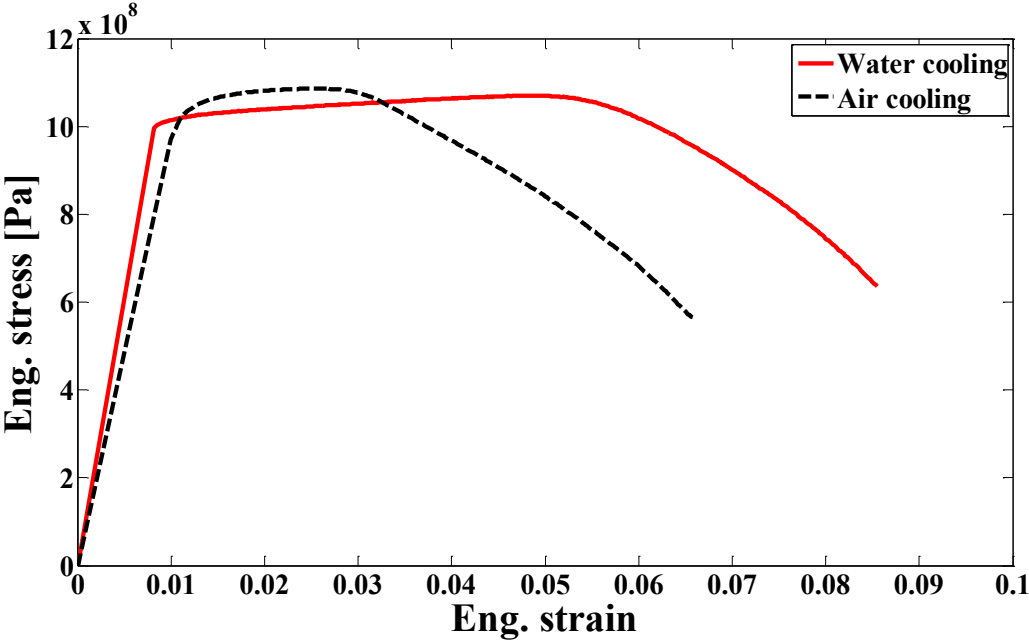


Figure 14. Typical engineering stress-strain curves of smooth PH 15-5 tensile specimens manufactured with and without water cooling. Both experiments were held with a constant cross head velocity of $2.64 [mm/min]$. (Nominal strain rate of $10^{-3} [1/s]$).

From Figure 14, one can notice a marked influence of the manufacturing process on smooth specimens, so that the local strain hardening caused in the notch is definitely a realistic issue.

Consequently, one may now simulate dynamic tensile tests of notched specimens, for which a slight variation of the mechanical properties in the notch vicinity is introduced.

The effect of small variations in the strain rate sensitivity were studied with the material parameters of case 1 ($a=6.7$, $\dot{\epsilon}_m = 5e6 [s^{-1}]$) and a fixed maximal velocity of $18.5 [m/s]$.

For that purpose an area with a radius of $130[\mu m]$ around the notch root was selected to have slightly different material properties than the rest of the specimen, as illustrated in Figure 15.

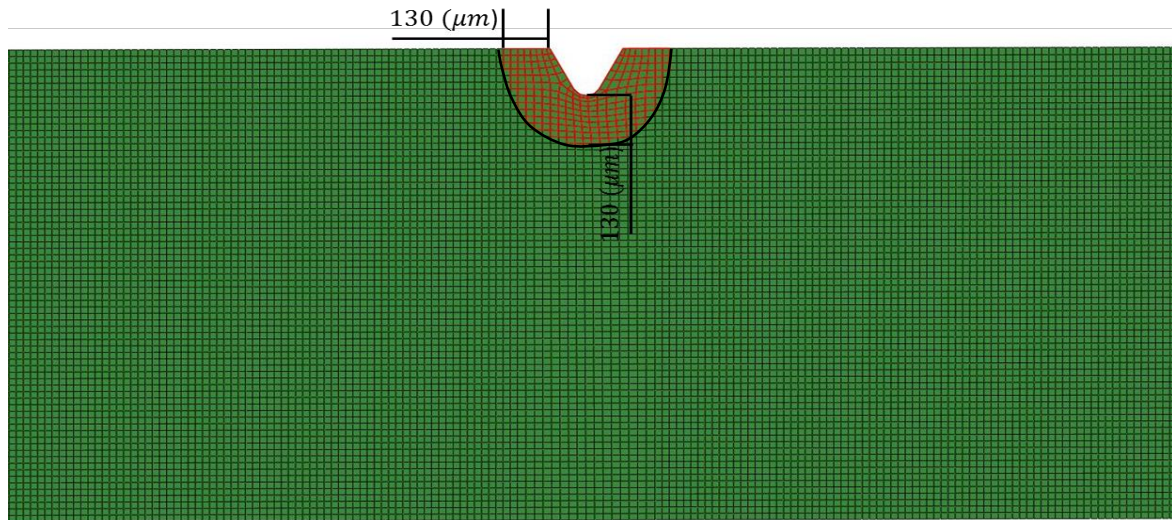


Figure 15. Part of the meshed specimen, with an area around the notch-tip that is influenced by the notch machining process.

The strain-rate hardening parameter at the lower strain rate regime, denoted by m , was taken to be m_{notch} in the notch, surrounded by m_{nom} at a distance greater than $130[\mu m]$. The value of m_{notch} was systematically increased from m_{nom} until a value was found for which the geometrical necking site became dominant in the failure process, meaning that the U_1 values at the potential failure location meet, just as shown in Figure 11 c.

In the studied case (case 1), defined by ($a=6.7$, $\dot{\epsilon}_m = 5e6[s^{-1}]$), the strain rate hardening exponent in the vicinity of the notch-tip was varied in the range $m_{notch} = 0.012, 0.015, 0.017$ and 0.020 .

Figure 16 shows the flow stress at $\epsilon_p = 0.4$ as a function of the strain rate for both m_{notch} (around the notch) and m_{nom} (rest of the specimen).

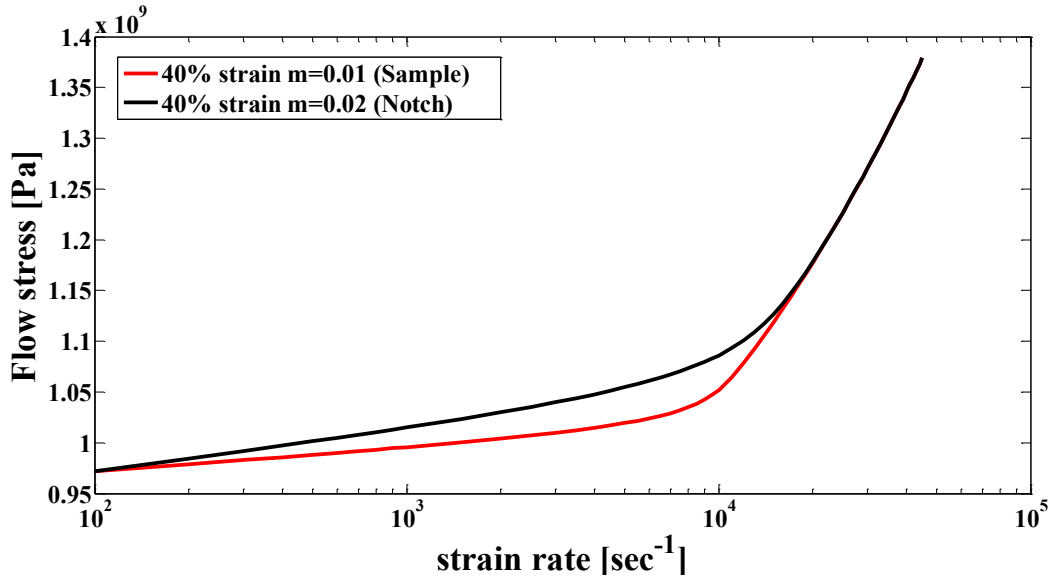


Figure 16. Flow stress at $\varepsilon = 0.4$ as a function of the strain rate for case 1 parameters with different strain rate hardening exponents (m).

The maximum difference in stress between the notch and the rest of the specimen at $\varepsilon_p = 0.4$ and $m_{notch} = 0.02$, is $\Delta\sigma_{max} \approx 4.65\% = 48[MPa]$. For smaller examined values of m_{notch} , $\Delta\sigma_{max}$ is of course smaller.

In order to see the effect of the local hardening in the notch, the macroscopic elongation until the "meeting time" was recorded for each m_{notch} value, with a $V_{max} = 18.5[m/s]$. The change of the macroscopic elongation up to the "meeting time" for different values of the strain rate hardening in the notch surrounding is show in Figure17.

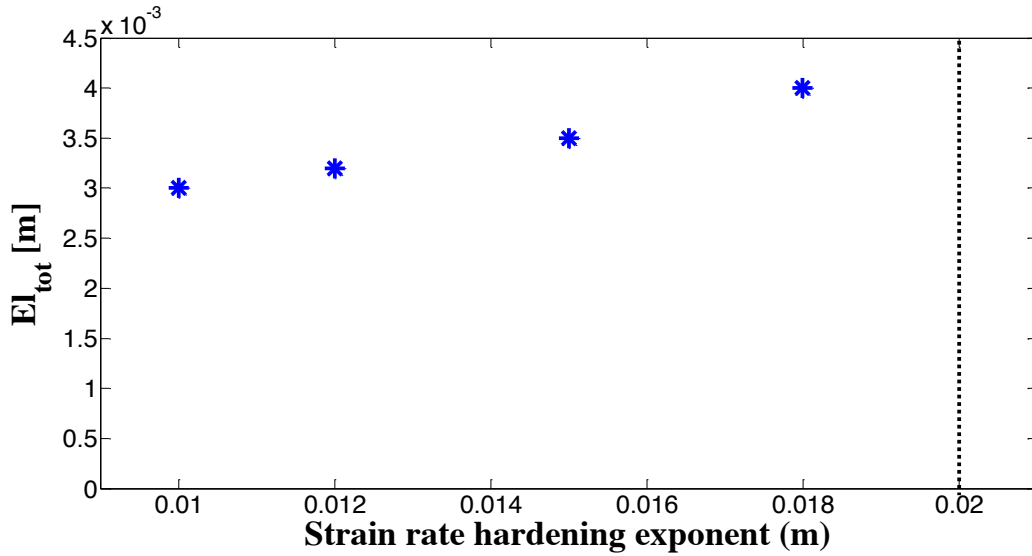


Figure 17. The nominal elongation of the specimen at the meeting time for $V_{max} = 18.5 [m/s]$, for different values of strain rate hardening in the notch vicinity. Note that for $m=0.02$, there is no meeting point as the neck dominates throughout the process.

According to Figure 17 the machining process plays a significant role in the competition between the potential failure sites. When the notch area is more hardened, the sample elongates more before reaching to its final failure state, indicating that the notch is less dominant in the competition between the potential sites. In addition, a change of less than 4.65% in the nominal flow stress ($m_{notch} = 0.02$), is sufficient to cause a shift in the failure locus. Therefore one can suggest that minor perturbations in the material flow stress can cause a significant change in the overall structural response of the stretched sample.

Discussion

This research was primarily motivated by the experimental observation of more than 130 specimens, for all of which, even in the presence of a significant structural imperfection, the dynamic failure locus (neck) was identical to that of a smooth (flawless) specimen. It was also observed in most cases that the dynamic failure locus was determined by the applied boundary conditions and not by the geometrical imperfection.

We carried out a systematic investigation of the main factors who might dictate this behavior, namely inertial effects, boundary conditions and the material response to high strain rate. In doing so, we tried to separate the structural effects from the material ones, keeping in mind that boundary conditions and material response are inherently coupled through the material's rate sensitivity and strain-rate hardening.

A first outcome of this research is that the velocity amplitude of the applied boundary condition is a determinant factor indicating the failure locus, a fact that is already known to some extent since Von Karman and Duwez's seminal contribution [26]. However, while this work addressed infinitely long rods, our work investigated finite length specimens. In the range of the low applied velocities, the failure locus is apparently determined by the imperfection without any significant competition from another potential failure site. Increasing of the velocity reveals a competition between the existing imperfection and a potentially developing neck on the impacted side of the specimen. As the velocity is further increased, the imperfection (notch) becomes insignificant and is simply "ignored" as a potential failure locus.

To characterize this competition between potential failure loci, we used numerical simulations, and chose to monitor the radial growth rate (evolution) of the two competing failure sites. This appears to be the most natural choice of a quantitative measure describing the imperfection growth in our case.

A second outcome of this investigation is that the high-rate mechanical response of the tested material has an effect that is similar to that of the increased velocity. For that, it is sufficient to note that the vicinity of the notch-tip experiences very large strain rates. This has a significant effect on the local flow stress for a material that is strain-rate sensitive. From there on, if the local stress elevation is sufficiently high, other cross-sections of the specimen will be

increasingly loaded. In fact, this effect just counteracts the stress-concentration effect of a notch, of which one would intuitively expect it is always predominant in a structure.

This point was systematically investigated through a series of simulations in which the parameters representing the material strain-rate hardening were varied, for a smooth specimen. And it was indeed observed, as mentioned earlier, that the failure locus (neck) would develop outside the notch area. It was thus observed that the more rate-hardening the material, the more resistant the specimen to plastic localization, together with necking in a different location along the gauge, close to the impacted side.

This notion was further extended to the case where local strain hardening of the notch due to the machining process is considered. Generally, such effects are not systematically taken into account, but in the present case it was especially interesting to investigate the extent to which a small variation in the local mechanical properties of the material can affect the overall structural response, in view of the above. It was indeed observed that, changing the strain rate hardening sensitivity in a manner which yields a small variation in the flow stress (less than 5%) in the immediate vicinity of the notch is sufficient to trigger the observed failure pattern outside the notch.

It is felt that, while the present results are physically sound to an extent they explain the respective influence of the boundary conditions and the material properties on the failure locus transition, the phenomenon in itself is rather counter-intuitive. Engineering common sense would suggest that a notch, thus a stress concentration, would always dictate the failure locus of a tensile specimen. While this is true in the quasi-static regime, this is no longer the general case in the dynamic regime. Such an observation, its modeling and comprehension, all have applications in the engineering design realm. Likewise, the obtained results clearly show and explain that under the given circumstances, a stress concentration discontinuity may not

be of major concern for the design of dynamically tensed structures. The present work provides both an approach and the tools to analyze and comprehend the phenomenon.

Conclusions

We have presented here a hybrid experimental-numerical study of the response of a flawed structure to a dynamic tensile load. The results, that are counter-intuitive with respect to the quasi-static perspective, show numerous instances where failure will not initiate from the flaw. This study shows that the locus of dynamic tensile failure of a flawed (notched) structure is dictated by several factors. The first, of course, is the applied velocity as a boundary condition, whose influence is so dominant that it overcomes the presence of the flaw. Next, the strain-rate sensitivity, and rate-hardening of the material, all play a role by locally toughening the notch area to an extent that the latter no longer acts as a "weak link". In fact, it was shown that at sufficiently high velocities, the very high local strain rates in the notch vicinity counteract the deformation and transfer the load to another part of the specimen which ultimately grows a neck there.

Finally, from a practical design perspective, the dynamic mechanical properties and boundary conditions should both be carefully taken into account when designing a tensile notched structural component, with a controlled failure locus.

Acknowledgement

The authors acknowledge with pleasure Prof. J.A. Rodriguez-Martinez and Prof. A. Needleman for many interesting discussions and suggestions. Mr. A. Godinger is acknowledged for his dedicated technical assistance.

References

- 1 Norton RL. (2004) Design of machinery: an introduction to the synthesis and analysis of mechanisms and machines, McGraw-Hill.
- 2 Roark RJ, Young WC. (1975) Formulas for stress and strain, McGraw-Hill.
- 3 Budynas RG, Nisbett JK. (2008) Shigley's mechanical engineering design, McGraw-Hill New York.
- 4 Inglis C. (1997) Stresses in a plate due to the presence of cracks and sharp corners. SPIE MILESTONE SERIES MS,137: 3-17.
- 5 Coker E, Chakko K, Satake Y. (1919) Photoelastic and strain measurements of the effects of circular holes on the distribution of stress in tension members. Proc Inst Eng Shipbuilding Scotland,63: 34-94.
- 6 Howland R. (1930) On the stresses in the neighbourhood of a circular hole in a strip under tension. Philosophical Transactions of the Royal Society of London Series A, Containing Papers of a Mathematical or Physical Character: 49-86.
- 7 Strandberg M. (2001) Upper bounds for the notch intensity factor for some geometries and their use in general interpolation formulae. Engineering fracture mechanics,68: 577-585.
- 8 Zappalorto M, Lazzarin P. (2011) Strain energy-based evaluations of plastic notch stress intensity factors at pointed V-notches under tension. Engineering fracture mechanics,78: 2691-2706.
- 9 James W, North W. (1969) Dynamic stress concentration using the photoelastic technique. J Strain Anal,4: 261-266.
- 10 Nakayama N, Ohashi M, Takeishi H. (1998) Dynamic stress concentration in a strip plate with fillet. JSME international journal Series A, Solid mechanics and material engineering.326-331 :41,
- 11 MATSUMOTO H, ADACHI T, KAKUHAMA Y, FUKUZAWA K. (1990) Analysis of the dynamic stress concentration factor by the two-dimensional boundary element method. JSME international journal Ser 1, Solid mechanics, strength of materials,33: 37-43.
- 12 Osovski S, Rittel D, Rodríguez-Martínez JA, Zaera R. (2013) Dynamic tensile necking: influence of specimen geometry and boundary conditions. Mechanics of Materials.
- 13 Rittel D, Rotbaum Y, Rodríguez-Martínez J, Sory D, Zaera R. (2014) Dynamic necking of notched tensile bars: an experimental study. Experimental Mechanics: 1-11.
- 14 El Maï S, Mercier S, Petit J, Molinari A. (2014) An extension of the linear stability analysis for the prediction of multiple necking during dynamic extension of round bar. International Journal of Solids and Structures,51: 3491-3507.
- 15 Kolsky H. An investigation of the mechanical properties of materials at very high rates of loading. pp. 676. IOP Publishing (1949.)
- 16 Harding J, Wood EO, Campbell JD. Tensile testing of materials at impact rates of strain. pp. 88-96. SAGE Publications (1960.)
- 17 Hibbett, Karlsson, Sorensen, Hibbitt. (1998) ABAQUS/standard: User's Manual, Hibbitt, Karlsson & Sorensen.
- 18 Zhou M, Needleman A, Clifton RJ. (1994) Finite element simulations of shear localization in plate impact. Journal of the Mechanics and Physics of Solids,42: 423-458.

- 19 Hertzberg RW. (1996) Deformation and fracture mechanics of engineering materials, Wiley New York.
- 20 Tetelman AS, McEvily AJ. (1967) Fracture of structural materials, Wiley New York.
- 21 Rotbaum Y, Rittel D. (2014) Is There An Optimal Gauge Length for Dynamic Tensile Specimens? *Experimental Mechanics*,54: 1-10.
- 22 Freund L, Hutchinson J. (1985) High strain-rate crack growth in rate-dependent plastic solids. *Journal of the Mechanics and Physics of Solids*,33: 169-191.
- 23 Hutchinson J, Obrecht H. (1977) Tensile instabilities in strain-rate dependent materials. *Proc of Fracture 1977, ICF4*.
- 24 Ghosh A. (1977) Tensile instability and necking in materials with strain hardening and strain-rate hardening. *Acta Metallurgica*,25: 1413-1424.
- 25 Regazzoni G, Johnson J, Follansbee P. (1986) Theoretical study of the dynamic tensile test. *Journal of Applied Mechanics*,53: 519-528.
- 26 Von Karman T, Duwez P. (1950) The propagation of plastic deformation in solids. *Journal of Applied Physics*,21: 987-994.